A synthetic spring-neap tidal cycle for long-term morphodynamic models

R.A. Schrijvershof[1,2], D.S. van Maren[3,2,4], P.J.J.F Torfs[1], A.J.F. Hoitink[1]

[1]Wageningen University & Research, Environmental Sciences Group, Wageningen, The Netherlands
[2]Deltares, Delft, The Netherlands
[3]State Key Lab of Estuarine and Coastal Research, East China Normal University, Shanghai, China
[4]Delft University of Technology, Faculty of Civil Engineering and Geosciences, The Netherlands

Key Points:

- A new approach to devise periodic tidal boundary conditions for long-term morphodynamic simulations is developed
- The new method better represents tidal water level dynamics, bed shear stress, and residual sand transport
- The pros and cons of both the new and existing approaches are evaluated

Corresponding author: R.A. Schrijvershof, `reinier.schrijvershof@wur.nl`

Abstract

Existing tidal input reduction approaches applied in accelerated morphodynamic simulations aim to capture the dominant tidal forces in a single or double representative tidal cycle, often referred to as a "morphological tide". These heavily simplified tidal signals fail to represent the tidal extremes, and hence poorly allow to represent hydrodynamics above the intertidal areas. Here, a generic method is developed to construct a synthetic spring-neap tidal cycle that (1) represents the original signal; (2) is exactly periodic; and (3) is constructed directly from full-complexity boundary information. The starting point is a fortnightly modulation of the semi-diurnal tide to represent spring-neap variation, while conserving periodicity. Diurnal tides and higher harmonics of the semi-diurnal tide are included to represent the asymmetry of the tide. The amplitudes and phases are then adjusted to give a best fit to histograms of water levels and water level gradients. A depth-averaged model of the Ems estuary (The Netherlands) demonstrates the effects of alternative tidal input reduction techniques. Adopting the new approach, the shape of the tidal wave is well-represented over the entire length of the estuary, leading to an improved representation of extreme tidal conditions. In particular, representing intertidal dynamics benefits from the new approach, which is reflected by hydrodynamics and residual sand transport patterns that approach non-schematized tidal dynamics. Future morphodynamic simulations forced with the synthetic signal are expected to show a more realistic exchange of sediment between the channels and tidal flats, likely improving their overall predictive capacity.

Plain Language Summary

The time-scales of erosion and deposition processes in estuaries and tidal basins are several orders of magnitude larger than the time scales of the changing flows (years versus hours, respectively). To efficiently simulate years of erosion and deposition, an acceleration factor is applied to estuarine and coastal models that simulate the long-term bed level developments. Tidal information used to force these accelerated models at the seaward boundary requires an exactly repetitive signal to avoid inconsistencies in the upscaling approach. A tidal input reduction technique is required to cope with the fact that successive spring-neap cycles are never identical. In this paper, a tidal input reduction method is developed that yields a synthetic, periodic tidal signal representing the variation of amplitudes and asymmetries present in a multiyear tidal signal. These variations are not captured well in existing, more limited, approaches for tidal input reduction. The results from a numerical model forced with the synthetic tidal signal shows that intertidal dynamics and residual sand transports are simulated more realistically, compared to existing approaches. The new tidal input reduction method should improve the exchange between the channels and intertidal areas in long-term estuarine and coastal models, presumably allowing for a more realistic assessment of erosion and deposition in these areas.

1 Introduction

The long-term or multi-decadal evolution of estuaries and tidal basins is largely controlled by the interaction between hydrodynamic forcing and the sediment bed (De Swart & Zimmerman, 2009). This morphodynamic dependence on hydrodynamic controls allows for a quantitative investigation on the evolution of tidal basins using process-based numerical models. Such morphodynamic tools in turn allow to simulate the evolution of deltaic environments, which are increasingly influenced by anthropogenic impacts (Syvitski et al., 2009) jeopardizing ecosystem services and potentially leading to morphological instability (Hoitink et al., 2020). Although numerical bed evolution models are often developed to predict the direct morphological response to engineering measures (De Vriend et al., 1993), they appear to be more realistic when the time scales related to the investigated changes (T_c) and the time-scale at which the model attains dynamic equilibrium (T_e) are longer (Dam et al., 2016). Often, the developments from the initial conditions towards the model's dynamic equilibrium obscure the morphodynamic impact of the interventions where the model was originally designed for. As a consequence, process-based models are increasingly used to investigate not only decadal but also centennial and even millennial morphological evolution of estuarine and tidal environments (e.g.; Dastgheib et al., 2008; Van der Wegen & Roelvink, 2012; Nnafie et al., 2018; Braat et al., 2017).

Long-term morphodynamic modelling requires appropriate up-scaling of the effects of hydrodynamic processes that typically fluctuate within hours or days to the time periods relevant for morphological changes. Various techniques exist to reduce the computational costs for the slow bed level evolution, while accounting for the shorter hydrodynamic variability. These techniques range from postponed morphological updating, based on gradients in the tide-averaged residual transport, to constructing simplified sediment balances that express bottom change in terms of sediment transport gradients depending only on the local water depth (Latteux, 1995; De Vriend et al., 1993; Roelvink, 2006; Roelvink & Reniers, 2011). The most commonly used morphological updating technique is the fully coupled approach (Roelvink, 2006), where the bed level is updated every hydrodynamic time step. Such continuous updating includes short-term interactions between flow, sediment transport, and morphology, resulting in a stable bed evolution, also in intertidal areas which are inundated during high water conditions only. From a physical point of view, the hydrodynamics should be resolved as detailed as possible. For reasons of computational efficiency, long-term morphological evolution is often modelled with the additional use of a so-called morphological timescale factor (or MorFac, MF), essentially a multiplication factor for the depth change (Roelvink & Reniers, 2011). At each hydrodynamic time step, the calculated bed level change is multiplied with this factor, reducing the required simulation time with a factor MF. This accelerated approach resolves morphodynamic processes operating at intratidal timescales, while maintaining the speed, stability, and accuracy of tidally averaged updating approaches (Van der Wegen et al., 2008). In idealized geometric configurations, the MF approach can produce stable bed evolution patterns for values up to $O(1000)$ that do not deviate significantly to the patterns simulated with smaller values of MF. A pre-requisite for stability is that the bed level changes are small compared to water depth, so that no irreversible changes develop within a phase of the tidal cycle (Van der Wegen & Roelvink, 2008).

Accelerated long-term simulations require schematized boundary conditions with limited extremes, because the sediment transport fields for bed level adaptation are extrapolated with the MF approach (and may not exceed critical values within a computational timestep). The time-series of boundary conditions need to be represented by a reduced number of conditions consisting of a repetitive pattern that includes the dominant forcing conditions, but excludes intermittent events (e.g. storms) that may exaggerate the bed evolution. The goal of input reduction is therefore to derive a limited representative subset of forcing conditions that approach the residual transport and associated morphological change patterns compared to a simulation forced with the full time-series over the period of interest (i.e. a 'brute-force' simulation).

Existing methods for tidal input reduction aim at capturing the dominant tidal dynamics in a single tide (e.g.: Dastgheib et al., 2008; Van Maanen et al., 2013) or with two representative tidal cycles (e.g.: Latteux, 1995; Lesser, 2009). Such simplified tidal signals have been shown to reasonably reproduce morphological changes of tidal channels (Van der Wegen & Roelvink, 2012; Van Der Wegen et al., 2011; Dissanayake et al., 2009; Dastgheib et al., 2008). However, heavily simplified tidal signals fail to represent the tidal extremes (the tidal elevation above Mean High Water and below Mean Low Water), because they neglect these variations. They poorly represent intertidal areas, which exert a major impact on the development of tidal asymmetry (Friedrichs & Aubrey, 1988). Although the tide-averaged transport of non-cohesive sediments in the main estuarine channels is captured well with solely a semi-diurnal tide and relevant overtides (Van de Kreeke & Robaczewska, 1993), the long-term morphological development of tidal basins is driven by tidal asymmetries resulting from the combination of multiple tidal constituents (Guo et al., 2016). Preserving asymmetries present in the original tidal signal, as well as providing the hydrodynamic conditions necessary for the development of intertidal areas, is therefore a key requirement for the tidal input reduction approach. Despite its importance for long-term morphological modelling, the impact of tidal input reduction methods has rarely been systematically investigated.

A systematic investigation of tidal input reduction techniques preferably correlates such techniques to morphological output. However, morphological models are sensitive to parameterizations (e.g. the sediment transport formula) and settings (grid size, bed slope effect) used in the morphodynamic model (Van Maanen et al., 2011; Baar et al., 2019). Although the morphological output is steered by the simulated hydrodynamics, it is also strongly influenced by morphodynamic calibration parameters, diffusing the effect of the boundary schematization. In this paper we therefore refrain from morphodynamic simulations and focus on the effect of the tidal input reduction approach on hydrodynamic model parameters considered relevant for morphodynamics.

The aim of this paper is twofold. First, a tidal input reduction technique is introduced that yields a synthetic, periodic spring-neap tidal signal representing the tidal extremes as well as tidal asymmetry. Second, the effects of both existing and the new tidal input reduction approaches are systematically investigated, since such an evaluation is missing in the literature. Simulations forced with the original tidal signal (as a reference) and simulations forced with schematized tides are evaluated in terms of tidal asymmetry, bed shear stress, inundation of intertidal flats, and residual sand transports. For this latter purpose, we develop and apply a morphostatic (i.e. no bed level updating) model of the Ems estuary (The Netherlands).

The structure of the remainder of this paper is as follows. We first review existing tidal input reduction techniques and explain the new methodology (Section 2). We then develop a numerical model of a real-world estuary (The Ems estuary, Section 3) and apply this to examine the effect of various types of tidal input reduction techniques on simulated hydrodynamics and sand transport (Section 4). The implications of simplifying tidal signals are discussed in Section 5, and conclusions are drawn in Section 6.

2 Tidal input reduction

2.1 The morphological tide

The goal of tidal input reduction is to create simplified representative tidal boundary conditions for up-scaling bed level changes in process-based morphological models. The aim is to represent the original tidal series in a simplified signal in a sense that it produces the same residual transport or initial morphological change patterns for a defined period and region of interest. The simplified tide is constructed as a periodic signal, so that a sequence of the same synthetic tidal signals is continuous. Such a simplified tide is often referred to as the "morphological tide" (Latteux, 1995).

The most common method to derive a morphological tide can be summarised as follows (Roelvink & Reniers, 2011). The morphological development over a sufficiently long time period (e.g.: several spring-neap cycles) is executed with both full hydrodynamic forcing and with several accelerated simulations, each forced with a single tidal cycle, selected from the time-series. The simulated patterns of residual transport or bed level adaptations resulting from reduced input simulations and from the full forcing simulations are subsequently compared based on a correlation coefficient, and the slope of the regression. The tidal cycle that produces simulated results that best resemble the results from a full forcing simulation is then considered to be most representative.

Lesser (2009) demonstrated that such a simplified tide fails to correctly represent residual transport in some cases, because it neglects the asymmetry resulting from interaction between the main semi-diurnal constituent (M_2) and the main diurnal constituents (O_1 and K_1). Hoitink et al. (2003) demonstrated that in diurnal, or mixed mainly diurnal regimes a residual transport can develop resulting from the tidal asymmetry that arises from these primary constituents because they have angular frequencies that consist of sums and differences of two of the basic astronomical frequencies (see Pugh, 1987), leading to substantial residual transport and morphological changes (Van Maren et al., 2004; Van Maren & Gerritsen, 2012). In these regimes, the residual transport that arises from the triad interaction of K_1, O_1 and M_2 can be more important than the residual transport caused by the non-linear interaction of the main semi-diurnal component (M_2) with its first overtide (M_4) (Song et al., 2011), often considered to be the dominant mechanism for shallow water tides (e.g., Friedrichs & Aubrey, 1988; Van de Kreeke & Robaczewska, 1993). Lesser (2009) therefore included this triad interaction by defining an artificial constituent C_1 with half the frequency of the M_2 tidal constituent. The resulting *double tide* consists of C_1, M_2 and its overtides, and may include an additional scaling factor for the amplitude of M_2 and/or C_1, to account for the presence of a residual flow.

A literature review on publications that apply online-updated accelerated process-based morphodynamic models in tide-dominated settings was performed to provide an overview of current tidal forcing approaches (Table 1). The 40 publications reviewed reveal that tidal forcing is often reduced to the M_2 tidal constituent (17 publications). All of these studies comprise idealised model configurations. In modelling studies that give a more realistic representation of the estuarine environment, the tide is usually represented by M_2 and its overtides (4 publications), the empirically derived morphological tide (2 publications), or the morphological *double tide* (4 publications). These studies aim at capturing the dominant tidal forces in a single or double representative tidal cycle. However, the (1D) simulated long-term morphodynamic development of estuarine environments is governed by the combined effects of asymmetries resulting from the interaction of multiple tidal constituents and river-tide interaction (Guo et al., 2016). Particularly, the omission of the S_2 constituent reduces the effects of river-tide interaction and tidal asymmetry, leading to an underestimation of tide-induced residual transport. Yet, the effects of ignoring significant constituents in simplified tides are not well studied for 2D morphodynamics. Presumably because of the unknown effects of oversimplifying tides in 2D morphodynamic simulations, the authors of 13 publications chose to overcome the considerations for tidal input reduction by forcing the full tide (Table 1). However, using this approach in accelerated simulations the morphodynamic time cannot accurately be interpreted, because the sum of the tidal periods imposed lacks periodicity. The interval for integration of the residual transport is inconsistent and therefore the transport is not accurately averaged over the tidal periods in the signal. These studies that did not apply tidal input reduction focused on decadal time-scales and such an imperfect sediment balance may be acceptable with small acceleration factors. For long-term (i.e. longer than decadal) simulations using larger acceleration factors, a simplified cyclic tide representing all significant tidal constituents (and therefore their interactions) would be an important advance over earlier simplified tides because (the interaction between) each significant tidal constituent plays a role in driving tidal residual transport, and therefore in morphodynamic development (Guo et al., 2016).

2.2 A synthetic representative signal

We aim to develop a generic method to construct a representative tidal signal that incorporates tidal extremes in a synthetic spring-neap cycle, while remaining periodic. The target synthetic spring-neap cycle: (1) sufficiently represents the original signal to preserve asymmetries; (2) is periodic, to ensure consistency in the start and end of consecutive cycles and to control the relative phasing with other types of forcings (e.g.: wind, waves, river discharge, ecology); and (3) is derived directly from the boundary informa-

Table 1. Tidal forcing approaches used in online-updated accelerated morphodynamic simulations.

Tidal forcing	Literature
M_2	Bolla Pittaluga et al. (2015), Braat et al. (2017), Elmilady et al. (2022, 2020), Geleynse et al. (2011), Guo et al. (2015), Hibma et al. (2003), Leonardi et al. (2013), Marciano et al. (2005), Nahon et al. (2012), Van der Wegen et al. (2010), Van der Wegen and Roelvink (2008), Van der Wegen et al. (2008), Van Maanen et al. (2013), Xie et al. (2017), Yu et al. (2014), Zhou et al. (2014)
M_2 + M_2 overtides	Dissanayake et al. (2009), Dastgheib et al. (2008), Nnafie et al. (2018), Nnafie et al. (2019)
Morphological tide	Chen et al. (2022), He et al. (2022)
Morph. double tide	Elmilady et al. (2019), Van Der Wegen et al. (2011), Van der Wegen and Roelvink (2012), Van der Wegen and Jaffe (2014)
Full tidal forcing	Dam et al. (2008), Dam et al. (2016), Ganju and Schoellhamer (2010), Ganju et al. (2011), Ganju et al. (2009), George et al. (2012), Luan et al. (2017), Styles et al. (2016), Van der Wegen and Jaffe (2013), Van der Wegen et al. (2017), Weisscher et al. (2022), Zhang and Mao (2015), Zheng et al. (2021)

tion, to avoid the empirical procedure required for the *morphological tide*, which introduces a dependency on the parameters and the locations chosen for the analysis. The aim for the procedure is to provide a synthetic signal that resembles the original tidal signal, excluding variations resulting from non-tidal processes.

The construction of the synthetic signal starts with a fortnightly modulation of the amplitude of the semi-diurnal tide to represent spring-neap variations. A synthetic signal with the duration of a fortnight resembles more accurately the real-world amplitude and phase variation than a single or double tide. Higher harmonics of the semi-diurnal tide are included to represent the asymmetry of the tide. Diurnal tides are included, following the method of Lesser (2009) to account for the O_1-K_1-M_2 interaction while maintaining periodicity of the signal. The synthetic signal is given by:

$$\begin{aligned} \zeta(t) = \\ \left(\overline{A_{D_2}} + A_{D_{sn}} \cos(\omega_{sn} t)\right) \cos(\omega_{D_2} t - \phi_{D_2}) \\ + \overline{A_{D_4}} \cos(\omega_{D_4} t - \phi_{D_4}) \\ + \overline{A_{D_6}} \cos(\omega_{D_6} t - \phi_{D_6}) \\ + \overline{A_{D_8}} \cos(\omega_{D_8} t - \phi_{D_8}) \\ + \overline{A_{C_1}} \cos(\omega_{C_1} t - \phi_{C_1}) \end{aligned} \qquad (1)$$

where $A_{D,n}$ is the amplitude, $\omega_{D,n}$ the angular frequency, and $\phi_{D,n}$ the phase of the n^{th} tidal constituent. The angular frequency ω_{D_2} is taken equal to ω_{M_2}, and all other angular frequencies are an integer product or one over an integer product of this primary forcing frequency. The diurnal C_1 constituent has an amplitude of $\sqrt{2A_{O_1}A_{K_1}}$ and the phase average of ϕ_{O_1} and ϕ_{K_1}. The overbar denotes time-averaging and t is time. The amplitude of D_{sn} modulates $\overline{A_{D_2}}$ and is equal to the amplitude of the second largest peak in the semi-diurnal frequency band, which corresponds to S_2 or N_2. The length of the "morphological spring-neap cycle" we introduce is given by the closest even number (denoted by i) of D_2 cycles that fit into the length of the spring-neap period induced by M_2-S_2 interaction; exactly 28 semi-diurnal cycles. The angular frequency of the fortnightly modulation is then given by

$$\omega_{sn} = \frac{2\pi}{28 T_{D_2}} \tag{2}$$

where T_{D_2} is the period of the D_2 constituent.

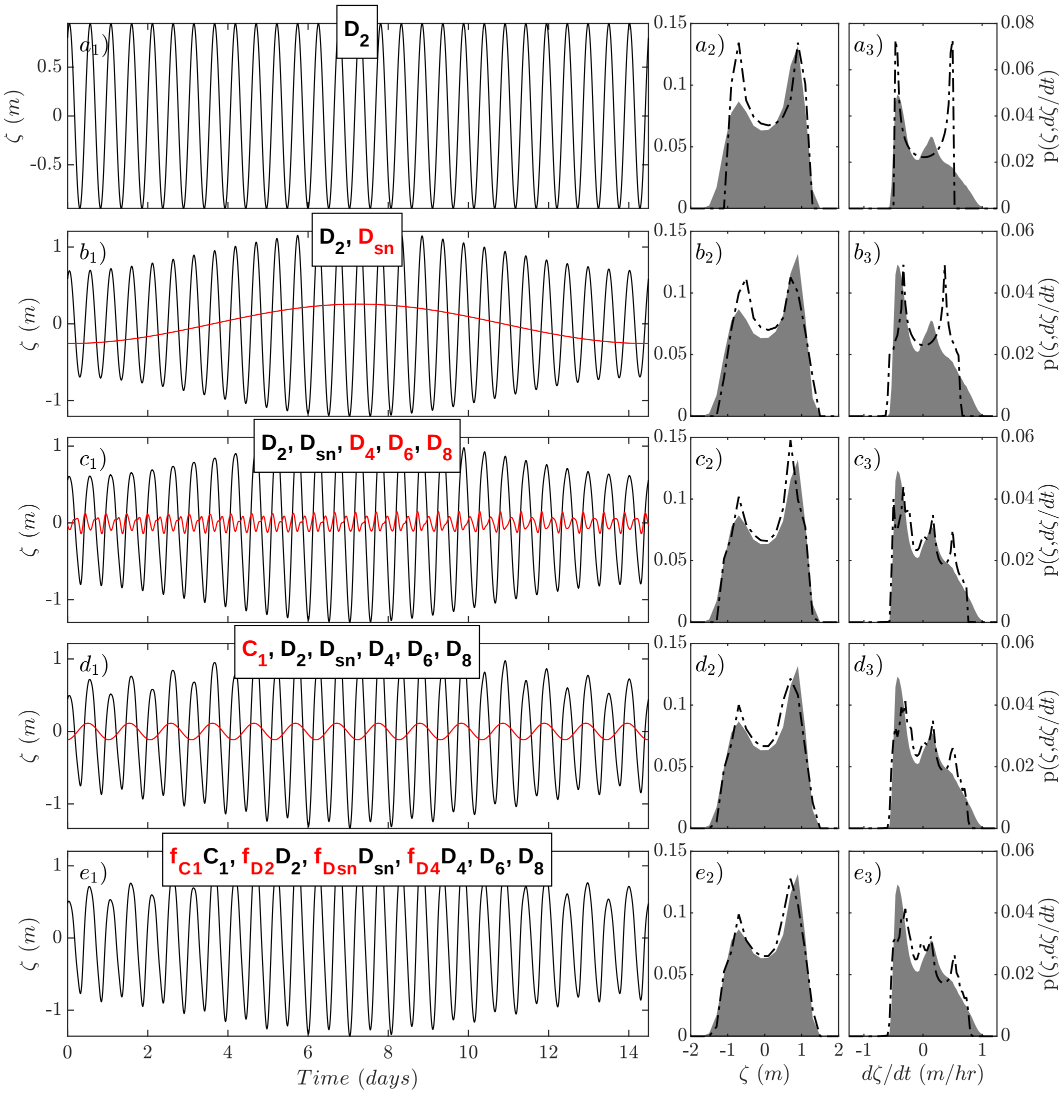

Figure 1. Step-wise construction of the synthetic spring-neap cycle, adding constituents in panel a-d, and scaling in panel e. For each step the resulting time-series (subscripted by 1) are shown in black and the added tidal constituent in red. The panels subscripted by 2 and 3 show the histograms of the synthetic signal (dashed line) and the full tidal signal (gray patch) for ζ and $d\zeta/dt$, respectively.

The step-wise construction of the morphological spring-neap cycle is illustrated in Figure 1, using a 19-year record of water level observations collected in the Dutch North Sea (monitoring station Wierumergronden). The synthetic signal is compared with the full tidal signal using histograms of the free surface elevation (ζ) and the surface level gradient ($d\zeta/dt$). The histogram of ζ indicates asymmetry in tidal peaks, i.e. tidal peak asymmetry, and the histogram of $d\zeta/dt$ indicates asymmetry in the duration of the rising and falling limbs of the surface elevation time-series. The latter is also referred to as tidal duration asymmetry and is highly relevant for the direction and magnitude of residual bed-load transport of non-cohesive sediment (Van de Kreeke & Robaczewska, 1993). This approach based on histograms concisely characterises tidal asymmetry resulting from the interaction of all constituents, in contrast to the harmonic method that characterises the asymmetry resulting from two or more interacting constituents. The histograms in Figure 1 illustrate how the addition of the individual terms of Equation 1 provide a signal that progressively better resembles the nearly complete tidal signal (reconstructed with 68 significant constituents resolved through harmonic analysis, see Pawlowicz et al. (2002)).

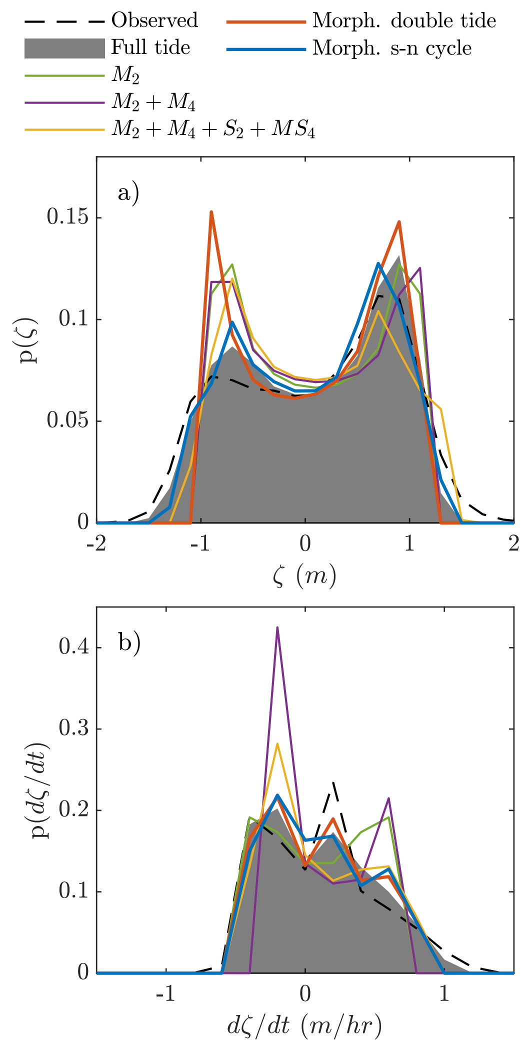

Figure 2. Histograms of ζ (a) and $d\zeta/dt$ (b) for the observed signal (dashed line), a tidal prediction including 68 resolvable tidal constituents (gray patch), and the simplified tidal signals (coloured) previously used for long-term morphological modelling. Histograms are constructed using a bin width of 0.2 m and $\frac{1}{6}$ m/hr for the the histogram of ζ and $d\zeta/dt$, respectively.

Applying basic trigonometry, the synthetic signal is rewritten as a linear combination of sines and cosines with zero phases, which facilitates the optimisation. This equation is fitted to the full astronomical tidal signal using scale factors to the amplitudes of the sines and cosines of D_2, D_{sn}, C_1, and D_4 (higher harmonics of D_2 are not scaled because of time efficiency in the algorithm). A combined Root-Mean-Squared-Error (RMSE) for the histogram of ζ and $d\zeta/dt$ is computed for each individual scaling factor. The error values are stored in a matrix to optimise the combination of scaling factors for the amplitudes of each tidal constituent.

Histograms of (1) the observed water levels at monitoring station Wierumergronden, (2) water levels from a full tidal reconstruction, and (3) water levels from the synthetic spring-neap cycle and other simplified tidal signals are shown in Figure 2. Representing the full tide with a single M_2 constituent clearly oversimplifies the signal as this M_2 tide is completely symmetric. Although this is slightly improved by adding an M_4 constituent, tidal extremes are not yet captured. These extremes are better represented when spring-neap variations (M_2+M_4+S_2+MS_4) are included, but the asymmetry of ζ is reversed. The morphological *double tide* represents the asymmetry of $d\zeta/dt$ well, but does not capture the extremes and asymmetry of ζ. The synthetic spring-neap cycle better approximates the extremes and asymmetries in the full tidal signal than the other simplified tides do. The synthetic signal does include, however, a third peak in the histogram of $d\zeta/dt$, which is not present in the full tide. Apparently, this peak is suppressed by tidal constituents other than included in the simplified tide.

3 Numerical model

3.1 Model set-up

A numerical model is developed to quantify how various tidal reduction techniques influence the spatial variation of hydrodynamics and sediment transport. The model is set up to represent a real-world estuary rather than an idealized case, because the complex topography of a realistic environment introduces tidal asymmetries to be represented appropriately. For this purpose we have selected the Ems estuary, a meso-tidal system on the Dutch-German border that is part the Wadden Sea. The tidal prism is predominantly accommodated by a single channel that aligns with the incoming tidal wave propagation direction, as the tidal wave travels from west to east along the North Sea coast. The discharge of the main river draining into the estuary (the Ems river) varies between 30 - 300 m^3/s, and is small compared to the flood tidal prism ($10^9 m^3$) (De Jonge et al., 2014). Other rivers discharging in the Ems estuary have a mean annual discharge that is smaller than 10 m^3/s.

The model is developed in the Delft3D Flexible Mesh model suite (Kernkamp et al., 2011). The numerical domain covers the offshore coastal part in the Wadden Sea, the estuary, and the river up to an up-estuary weir, with a grid cell size ranging from 1 km (offshore) to 30 m (Figure 3). The model is set-up in 2D depth-averaged (2Dh) mode, with corrections for spiral motion (secondary flow) applied to the depth-averaged momentum equations. Water level boundary conditions are derived from a validated hydrodynamic model that covers the Northwest European Shelf (Zijl & Groenenboom, 2019) for the years 2018-2019. Tidal constituents at the boundaries are adjusted according a comparison between modelled and observed amplitudes and phases, derived through harmonic analysis (Pawlowicz et al., 2002) at station Wierumergronden (close to the western boundary of the model - see Figure 3). A time-varying observed river discharge is prescribed at the upstream end of the Ems river for model calibration and validation, whereas a constant value (80 m^3/s for the Ems river and less than 10 m^3/s) for the smaller rivers) is prescribed for various scenario simulations. The bathymetry of the model is based on echosounding observations collected in 2014, which are made freely available by the Dutch Directorate-General for Public Works and Water Management.

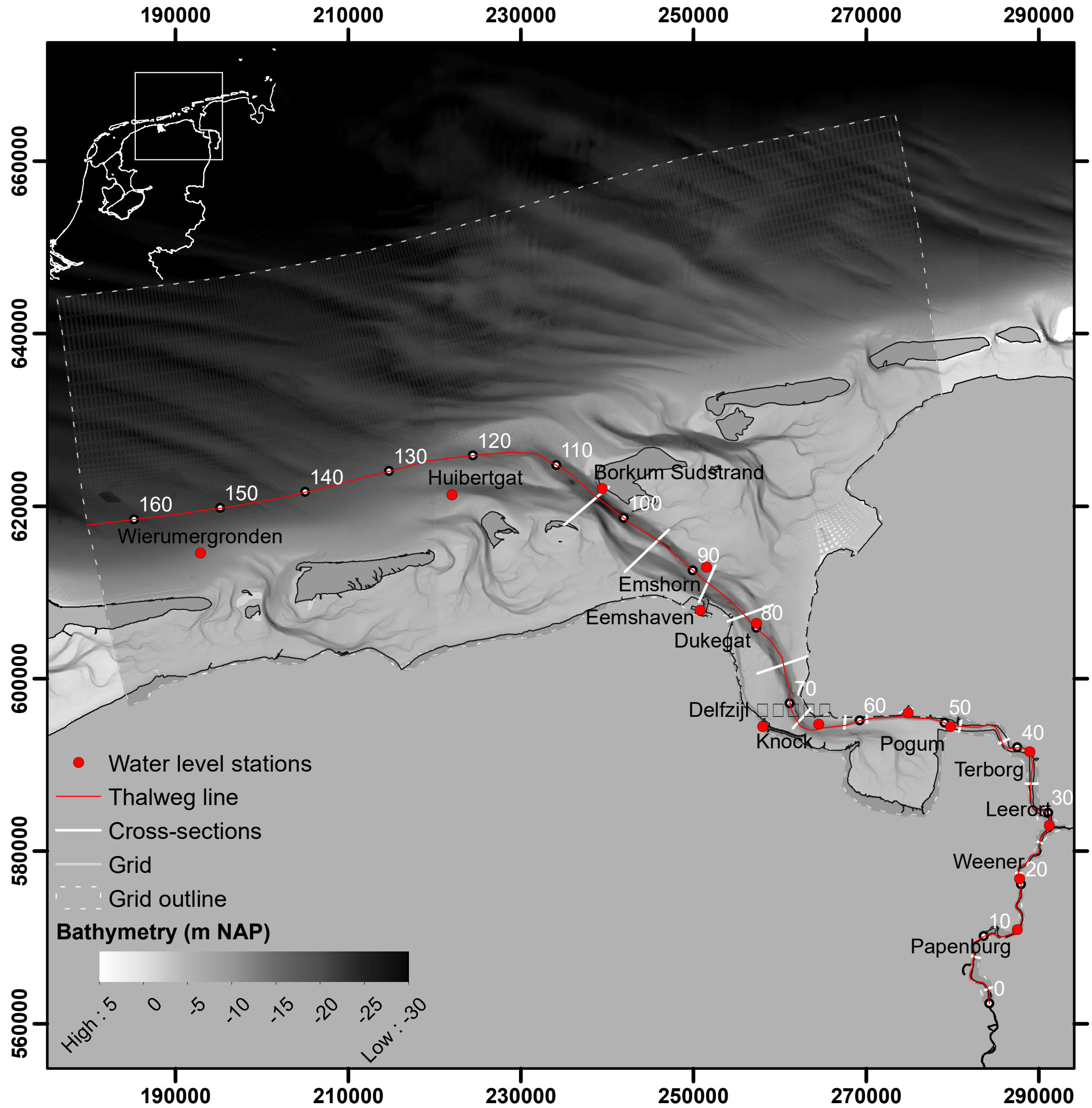

Figure 3. The Ems estuary and numerical model domain (gray lines), with the locations of water level observations (red dots) and a line that follows the main route of tidal propagation (red line) from the western boundary of the model through the thalweg of the estuary and river, with estuary kilometres defined with respect to the point of maximal tidal intrusion at the weir.

Sediment transport is computed with the Van Rijn (1993) formula for medium fine sand (180 μm). The model is executed in morphostatic mode (i.e. no bed update) because the feedback loops initiated by bed level adaptation complicates the analysis on the direct effects of the boundary schematization on hydrodynamics and residual transport. An equilibrium sand concentration is prescribed at the marine model boundaries, but no sand enters the model domain through the fluvial boundaries. There is interaction with the bed, which has an unlimited sand supply potential. The simulated sediment transports in the model can deviate significantly from the natural conditions. However, the settings for the sand transport model have a limited effect on the results because the simulations are used for a relative comparison between simulations with various boundary conditions.

3.2 Hydrodynamic calibration and validation

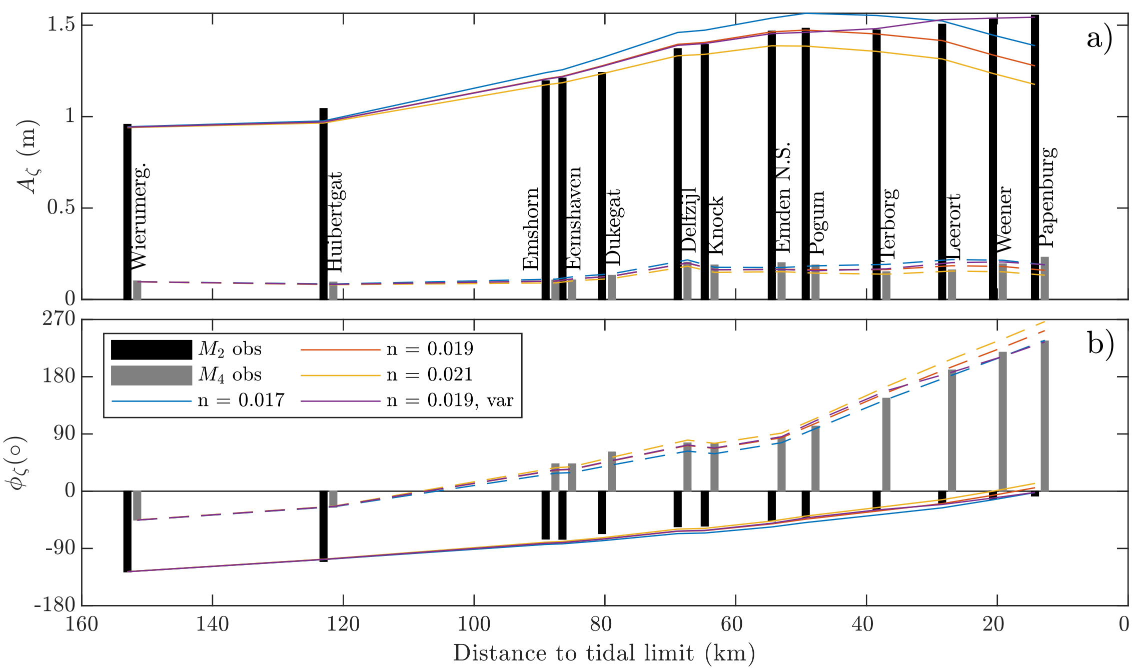

Figure 4. Observed and modelled amplitudes (a) and phases (b) of the M_2 and M_4 tidal constituents, based on the 2018 simulation. Model results (coloured lines) show the effect of different values for a spatially uniform Mannings' n ($m^{1/3}$ s^{-1}) and the best calibrated model with a spatially varying roughness in the Ems river.

Water level observations for the years 2018 - 2019 collected throughout the estuary are used to calibrate and validate the model (see Figure 3). The time-series are decomposed into tidal constituent amplitudes and phases using harmonic analysis (Pawlowicz et al., 2002). In the calibration phase, the model simulates the year 2018, using a spatially uniform roughness coefficient, Mannings' n, amounting to 0.017, 0.019, and 0.021 $m^{1/3}$ s^{-1} (Figure 4). Tidal propagation is best represented by a Manning's n value of 0.019 $m^{1/3}$ s^{-1}. Such a bed roughness, however, overestimates dampening of the tide in the Ems river. In reality, the tides amplify as a result of extensive fluid mud deposits in the Ems River, resulting in an apparent bed roughness around 0.10 $m^{1/3}$ s^{-1} (Van Maren et al., 2015). A linear decrease in bed roughness (from 0.019 $m^{1/3}$ s^{-1} at the entrance of the river towards 0.011 $m^{1/3}$ s^{-1} at the upstream end at the weir) is therefore employed, which better represents the tidal dynamics.

The model was validated against water level observations over the first five months of 2019. The modelled amplitudes of the four primary tidal constituents (M_2, S_2, O_1, K_1) and M_4 are typically within 15% of the observed amplitudes (Figure 5a). The errors are larger (up to 28%) for the S_2 and M_4 tidal constituents in the landward part of the Ems river (Figure 5b). Modelled phases are typically within 10° of observations (Figure 5c), but the modelled phases of O_1 and especially K_1 differ more than 20° in the tidal river part (Figure 5d).

The calibrated model introduced herein serves to evaluate alternative tidal input reduction approaches for morphodynamic modelling. The non-schematized tidal boundary conditions (full tidal, providing a reference condition) and alternative simplified tidal

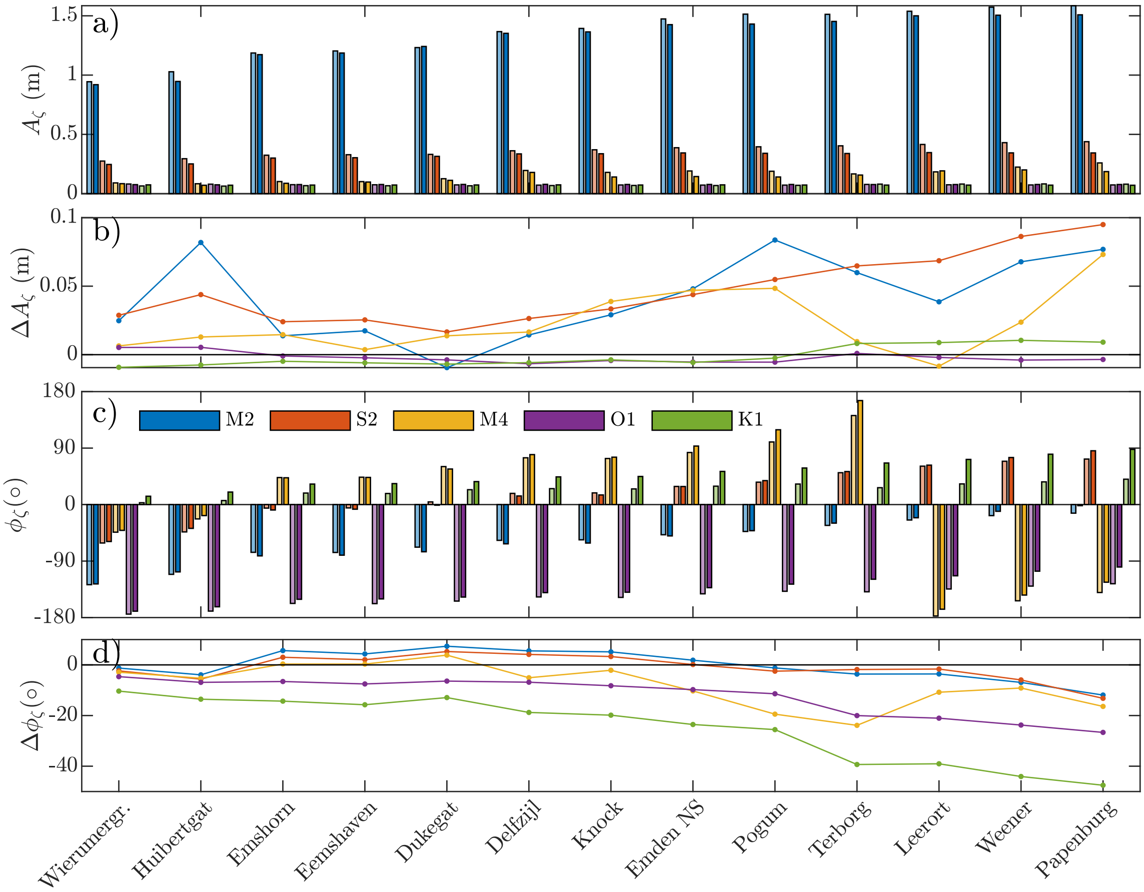

Figure 5. Observed (light coloured bars) and modelled (dark coloured bars) tidal constituent amplitudes (a) and phases (c), based on the 2019 simulation. The difference (observed - modelled) of the amplitudes and phases are shown in panels b and d, respectively.

representations (as in Figure 2) are detailed in Table 2. The boundary forcing with the morphological *double tide* includes an analytically derived scaling factor for M_2 (see Lesser (2009) for the derivation), to incorporate the total energy of the full tide (the sum of squares of the amplitudes of all tidal constituents) in the semi-diurnal frequency band. Applying the scaling factor, residual transports resulting from a mean (residual) flow is conserved in the simplified tide. The various tidal input reduction scenarios are compared to the reference in terms of tidal wave shape, bed shear stress, inundation, and sand transport in the following sections. All simulations (Table 2) are preceded by a two-week period that is excluded from the analysis to arrive at equilibrium conditions for the hydrodynamics and suspended sediment concentrations at the start of the analysis.

4 Results

4.1 Tidal wave shape

The representation of tidal wave shape is a primary indicator for the error made in the simulations forced with simplified tidal conditions. Figure 6 quantifies the adequacy of the tidal wave shape representation based on the RMSE between the tidal reduction scenario and the full tidal signal, for histograms of both ζ and $d\zeta/dt$. The fig-

Table 2. Duration of the simulations forced with simplified tidal signals and the full tidal simulation that serves as the reference. Simulation names are used in the legends of the figures in the results.

Simulation name	Duration
Full tidal	1 year
M_2	24 hr, 50 min
M_2M_4	24 hr, 50 min
$M_2M_4S_2MS_4$	14.77 days
Morph. double tide	24 hr, 50 min
Morph. spring-neap	14.48 days

ure clearly shows that only using an M_2 boundary forcing leads to the largest error. Including more tidal constituents in the boundary information decreases the error and introducing spring-neap variations ($M_2M_4S_2MS_4$) leads to a markedly better representation of tidal wave shape. The *morphological spring-neap tide* shows the smallest error, both for ζ and for $d\zeta/dt$. The improvement established by introducing spring-neap variations is largest in the coastal and central parts of the estuary (km 70 - 160), because error estimates for all tidal reduction techniques converge to the same value in the upper reaches of the estuary.

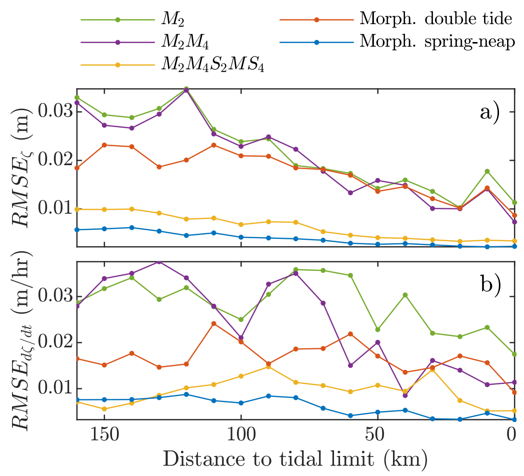

Figure 6. RMSE for the histogram of ζ (a) and $d\zeta/dt$ (b) between the simulations forced with simplified tides and the full tidal simulation, calculated at points in the thalweg along the estuary kilometres defined in Figure 3.

4.2 Bed shear stress

Maximum bed shear stress magnitudes along the estuary thalweg (Figure 7a) are most accurately represented when accounting for spring-neap variations, although there still is an underprediction of 30-40%. Including spring-neap variations gives a better representation of tidal wave shape, therefore, asymmetries are better preserved leading to higher maximum tidal velocities. The mean shear stresses in the thalweg (Figure 7b), on the other hand, are represented well by all simplified tides (although they are slightly overpredicted using the morphological *double tide*.). Maximum shear stresses are largest in the main tidal channels (Figure 8a) and, consequently, absolute improvements are largest in the tidal channels when accounting for spring-neap variations (compare in Figure 8 panel d and f to panel b, c, and e). However, maximum shear stresses on the intertidal areas are also underpredicted, in all simulated scenarios. An analysis on the error made in representing bed shear stress magnitudes over the complete model domain (presented in Figure 8) indicates that both the maximum (Figure 9a) and the mean (Figure 9b) shear stress magnitudes improve by incorporating tidal extremes. A reduction in RMSE is found in the subtidal (channels) and intertidal parts of the model domain. The consistent over-prediction of mean bed shear stress magnitudes with the morphological *double tide* in the thalweg (Figure 7b) is reflected by larger RMSE values in the subtidal domain (Figure 9b). Possibly, the overprediction is due to the implementation of a scaling factor for the M_2 tidal amplitude, to account for non-tidal energy in the spectral tidal frequency band.

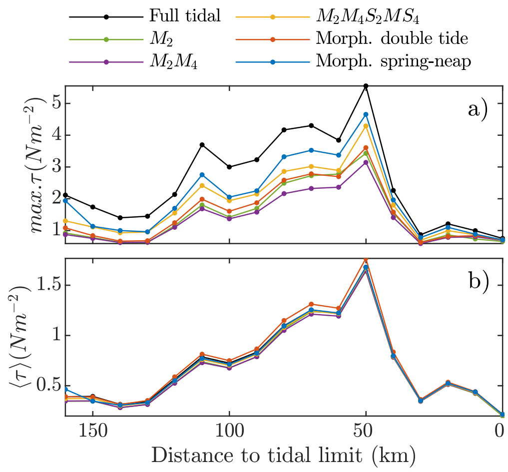

Figure 7. Maximum (a) and mean (b) bed shear stress magnitudes simulated with the full tidal forcing and simplified tides, calculated at points in the thalweg along the estuary kilometres defined in Figure 3.

4.3 Inundation

The intertidal areas, representated by computational cells that experience regular flooding and drying, make up ≈20% of the model domain. In those areas, the duration of inundation strongly controls sediment dynamics and therefore, the residence time of water over the tidal flats (Figure 10) is an important property to capture in morphological simulations of tidal environments. Particularly the high littoral zone (Figure 10a, b) is not captured by the simulations that exclude spring-neap variations, evidenced by too many computational cells that are permanently dry. Sediment cannot settle or erode in the higher intertidal parts when those areas never inundate. The bed level height of tidal flats will not be able to adjust to a height that resembles reality. Similarly, in the low littoral zone (Figure 10e, f), the simplified signals without spring-neap variations result in too many computational cells that are permanently inundated such that the lower intertidal zone becomes a subtidal area. Average conditions in the mid-littoral zone are well-represented by all simplified tides.

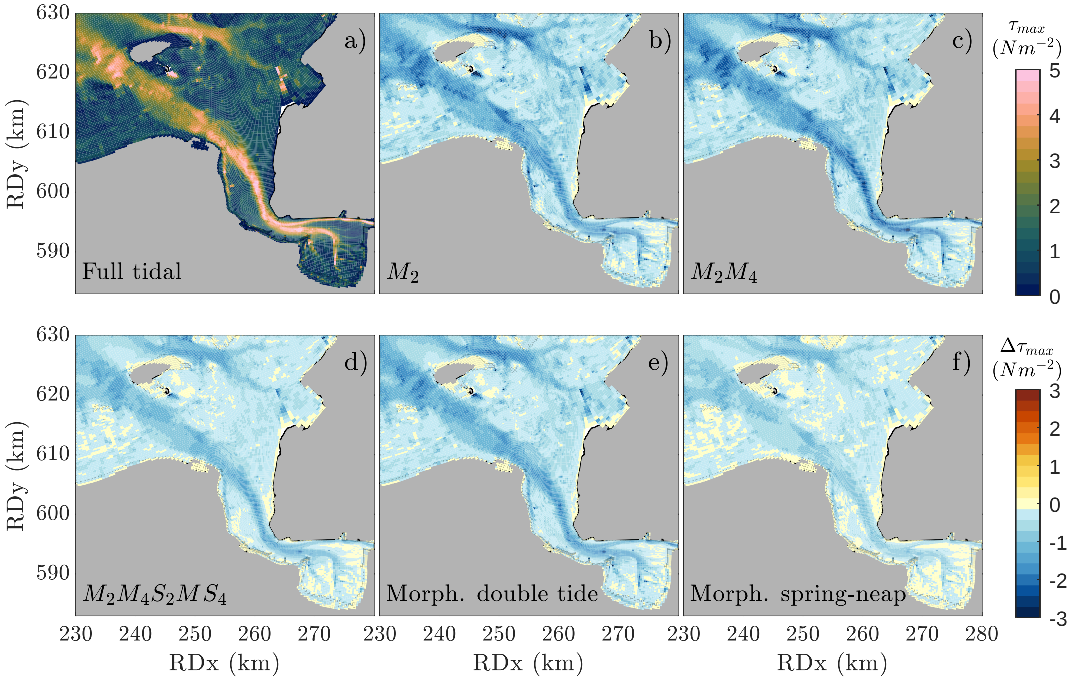

Figure 8. Maximum bed shear stress during the reference simulation (a) and difference in maximum bed shear stress between the scenarios and the reference (b-f)

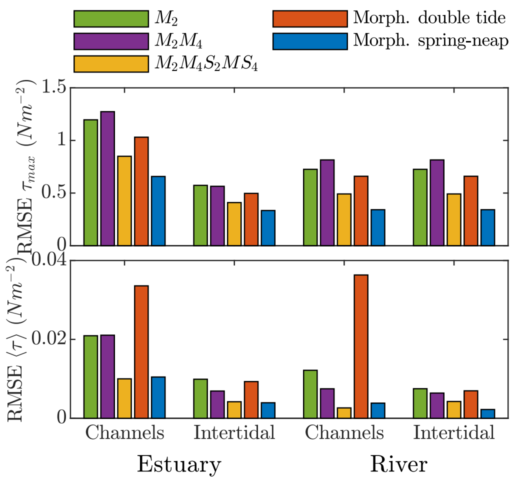

Figure 9. RMSE for the maximum (a) and mean (b) bed shear stress magnitudes between the simulations forced with simplified tides and the full tidal simulation. RMSE values are calculated as mean values for all the computational cells within the specified subregions estuary, river, subtidal channels and intertidal areas.

4.4 Sediment transport

The gross, cross-section integrated sand transport fluxes vary with each tidal cycle in the *full tidal* simulation. The mean of the range in gross transport flood fluxes (Fig-

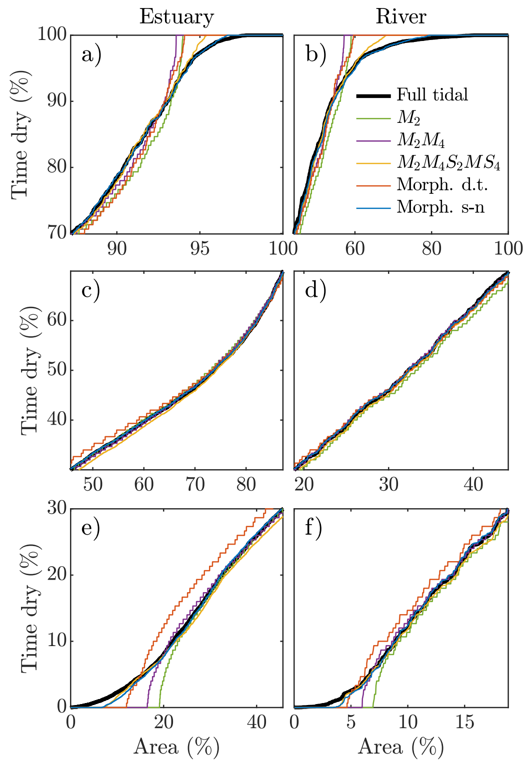

Figure 10. Cumulative distributions of the fraction of time of the total simulation length (in %) that a computational cell is dry (emerged), as a function of the fraction of the total intertidal area in the modelling domain. The distributions are shown for defined subregions; the estuary (a, c, e) and the river (b, d, f), and subdivided in the high (a, b), mid- (c, d), and lower (e, f) littoral zone.

ure 11a) is well-captured by the $M_2M_4S_2MS_4$ tide, the morphological *double tide*, and the morphological *spring-neap* simulations. The M_2 tide, the *morphological double tide*, and the *morphological spring-neap* simulations all reproduce the mean gross ebb transports reasonably well. For the full tidal simulation, the residual transport (Figure 11b) is flood-dominant at the mouth (km 85 - 108), ebb-dominant in the central part (km 45 - 85) of the estuary; and neither flood nor ebb dominant in the tidal river (km 0 - 45). This large-scale behaviour is captured well by each of the alternative simplified tides, except for the M_2 simulation, which prescribes a perfectly symmetric tide at the sea boundaries and therefore leads to an underestimation of the flood directed residual transport (Figure 11a). The morphological *spring-neap* tidal boundary conditions lead to residual transport best representing *full tidal* residual transport (Figure 11b). The M_2M_4 and $M_2M_4S_2MS_4$ tidal boundary conditions lead to an underestimation of the magnitude of the residual transport fluxes, and the *morphological double tide* generates slightly more ebb-dominant transport in the entire estuary.

The morphological evolution is not only driven by the magnitude of gradients in the residual transport flux, but also by the directions. An analysis of the error (RMSE) made in the direction and magnitude of residual transports averaged over all computational cells (Figure 12) reveals that particularly the error in direction is smaller for the simulations that include spring-neap variations. The RMSE for the magnitude of the residual transport shows less scatter, except for the M_2 simulations, which clearly deviates

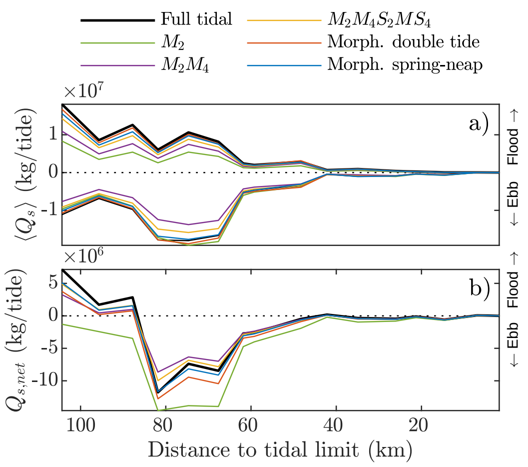

Figure 11. Mean of the total (bed + suspended) load gross transport fluxes (a) and residual transport per tidal cycle (b) in the thalweg (see the cross-sections in Figure 3 for locations).

in the channels. In general, including spring-neap variations reduces the error in magnitude and direction of residual transports in the channels and over the intertidal areas.

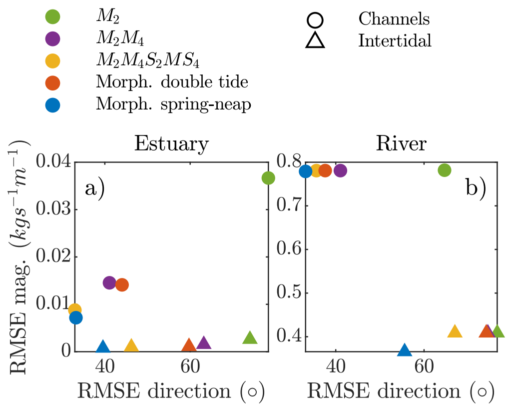

Figure 12. Error (RMSE) in the direction (horizontal axis) and magnitude (vertical axis) of the residual total (bed + suspended) load sand transport in the channels (circles) and on the intertidal areas (triangles).

5 Discussion

A new tidal input reduction method was developed which includes periodic spring-neap variation in a simplified tide. Prescribing this new method as boundary conditions in an estuarine setting improves the representation of tidal wave shape, maximum and mean bed shear stress magnitudes, inundation times, and residual sand transport patterns, compared to existing tidal input reduction methods to represent the non-schematized tidal dynamics. The strong and weak points of the new methodology and existing tidal input reduction techniques are summarised in Figure 13 using normalised scores, with 0 indicating a poor represention of the full tidal signal, and 1 indicating a full representation of the full signal. The scores are calculated as

$$score = \frac{z}{\max(z)}, z = 1 - \frac{x}{\max(x)} \tag{3}$$

The x-values for the parameters *Periodic* and *Deterministic* are binary (0 or 1), and *Cycle length* proceeds directly from Table 2. The other values for x are computed from the model scenario metrics presented in Chapter 4. An averaged RMSE between the output computed with a simplified and a full tide serves as x-value. The new method scores maximal on 10 out of 12 metrics, with lower scores only for the duration of the cycle and the duration of inundation (second-best score). Especially the scores computed from the various model scenarios strongly influence the morphodynamic evolution of a model (bed shear stress parameters, sand transport, inundation, and tidal asymmetry). When converting the model into morphodynamic mode, we therefore expect the new input reduction technique to provide physically more meaningful bed level predictions. However, as elaborated earlier, we do not explore the resulting morphodynamic impacts, which may be very case-specific and therefore cannot easily be generalized. The higher scores in Table 2 therefore motivate to replace traditional approaches for tidal input reduction with the new method.

The main drawback of the synthetic spring-neap cycle, following directly from Figure 13, is the simulation duration. The 28 M_2 cycles ($\approx$ 14.48 days) required in the computations is 14 times longer than the time required to simulate a cycle of the morphological *double tide* (Lesser, 2009). In practice this drawback is minor, because a shorter representative tidal period (e.g. the M_2 period) is usually frequently repeated. Simulating many tidal cycles is preferred because bed elevation changes over a single tidal cycle are small compared to inaccuracy, which are then linearly amplified by a comparatively large morphological upscale factor (MF). For this reason, a single morphological tidal cycle is repeated even more often than 28 times, up to multiple hydrodynamic years (e.g. Dastgheib et al., 2008). The longest acceptable hydrodynamic simulation time is then usually combined with the smallest possible MF because (too) large values for the MF can produce unrealistic bed development (Ranasinghe et al., 2011).

Numerical morphological models may also be forced with non-tidal processes, such as a seasonally varying river discharge (e.g. Van Der Wegen et al., 2011; He et al., 2022) or wave- and wind-driven re-suspension (e.g. Van der Wegen et al., 2017). Such non-tidal conditions are typically accelerated by a factor MF as well (i.e., an annual river flood recurs MF times per year). In these cases, the relative phasing of the various forcing factors with the tide need to be explicitly accounted for as well. Otherwise, for instance, persistently combining seasonal river floods or storm events with spring tide or flood conditions leads to biased bed development. In tidal series the M_2-S_2 phase differences throughout a spring-neap cycle differ for successive spring-neap cycles, which also holds for the phase differences between semi-diurnal and diurnal tides. In the synthetic spring-neap cycle, the relative phasing is identical for successive spring-neap cycles, which allows to optimize the relative phasing with non-tidal processes.

A tide-averaged transport for coarse sediment is generated by a representative tide consisting of a tide-induced Eulerian mean current (M_0), M_2 and any of its even overtides (Van de Kreeke & Robaczewska, 1993). When diurnal components are important, a similar net residual transport arises from the triad interaction of M_2-K_1-O_1 (Hoitink et al., 2003), which can be captured in a periodic double tide through an artificial diurnal component with half the frequency of M_2 (Lesser, 2009). Spring-neap variations are so far mainly ignored in representative tides (Dastgheib et al., 2008; Roelvink & Reniers, 2011). This paper demonstrates that simplified tides consisting of a single or a double tide (which are most frequently used for long-term morphological modelling) do perform well in representing mean bed shear stress and residual sand transports inside the estuarine channels. However, they fail to reproduce the full range of asymmetry in the tide leading to an underestimation of maximum bed shear stresses (controlling the timescales of bed level adaptation) and to represent the upper and lower intertidal inundation that steers the development of intertidal flats (Friedrichs, 2011). Representing the variation in tidal asymmetries is shown to be important to capture the residual sand transports on the intertidal flats as well. This is because the velocity skew (flood versus ebb dominance) over tidal flats is modulated during the spring-neap cycle (Nidzieko & Ralston, 2012). Therefore, if the intertidal areas are of insignificant importance in the environment studied and the focus of the study is on the tidal channels, ignoring spring-neap variations in a representative tide is presumably allowed. However, if the intertidal parts of the modelling domain are an integral part of the phenomena studied, morphodynamic models cannot suffice with a representative tide consisting of a *single* or *double tide*.

Applying the synthetic spring-neap cycle in a fully coupled morphodynamic model (including bed level adaptations) leads to much more realistic tidal dynamics. The computed residual sand transport will improve by including the tidal extremes and asymmetries resulting from the spring-neap modulations, promoting a more realistic channel transport and channel-shoal exchange. The inclusion of tidal extremes may also have negative effects, however. The resulting higher maximum bed shear stresses possibly limits the morphological acceleration factor, which can otherwise lead to unrealistic bed level developments. Such a potential shortcoming depends on various model settings (Reyns et al., 2014), and requires a case-specific analysis. Furthermore, the gross and net sand transport presented in this paper was based on simulations with a single fraction sediment bed existing of non-cohesive sediments, calculated with the Van Rijn (1993) formula. Multiple fraction sediment beds, including cohesive sediments, may develop unexpected interactions in conjunction with the synthetic spring-neap cycle which needs to be explored in a practical case. Planned long-term morphodynamic modelling will reveal the advantages and the challenges of the more realistic representation of tidal dynamics advocated in this paper.

6 Conclusions

Spring-neap variations can be included in simplified tidal signals that are applicable as boundary conditions in long-term morphological models. Compared to a single or a double tide, often used in morphodynamic simulations, tidal variation in a synthetic spring-neap cycle is better represented through a fortnightly modulation on the amplitude of the semi-diurnal tide. The tidal input reduction method developed in this paper yields a signal that: (1) resembles the amplitude variation of the full tidal signal and sufficiently preserves asymmetries to approach non-schematized tidal dynamics and residual sand transports; (2) is strictly periodic; and (3) can readily be derived from the full boundary conditions. It does not require a fitting procedure based on modelling results.

Process-based numerical models of tidal environments that include the tidal extremes induced by spring-neap variations represent the shape of the tidal wave through the tidal basin more realistically. Simulations with simplified tidal signals that neglect the tidal extremes underestimate maximum bed shear stresses in the channels and simulate a too

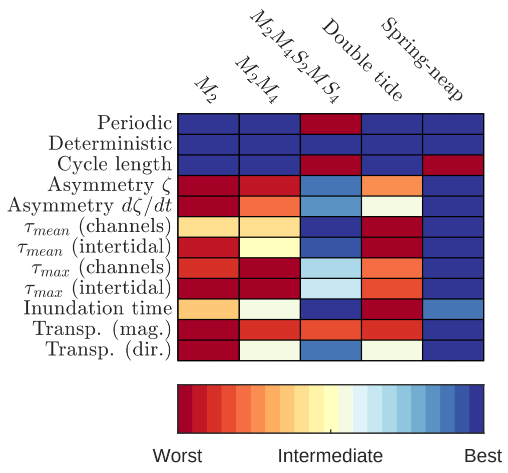

Figure 13. Normalised scores (0-1) for simplified tides to represent (simulated) non-schematized tidal conditions. The calculation of the score values is explained in the main text.

limited extent of the tidal flats. Although simulations forced with these signals approximate the tidally averaged residual sand transport patterns in the channels quite reasonably, an appropriate representation of the extremes is required to reproduce the patterns both in the channels and on the intertidal areas. The newly developed tidal input reduction method provides a signal that resolves non-cohesive sediment transport within the estuary more accurately, and may improve the simulated exchange of sediment between the channels and tidal flats.

7 Open Research

A toolbox is developed that allows to construct a synthetic spring-neap tidal cycle from a time-series of tidal elevations. The toolbox is developed in MATLAB code, and available for download at `https://github.com/Rschrijvershof/morphoSpringNeap.git`.

There are no restrictions on the data used in this study. The bathymetry data used for model set-up was requested through the servicedesk data of Rijkswaterstaat (`https://www.rijkswaterstaat.nl/formulieren/contactformulier-servicedesk-data`). Observed water level data from Dutch monitoring stations are available at `https://waterinfo.rws.nl` and the data from the German monitoring stations was requested at WSA Ems-Norsee (`https://www.wsa-ems-nordsee.wsv.de/`). The configurations of the numerical model simulations used in this article are stored at 4TU.ResearchData (`https://doi.org/10.4121/19845262.v1`).

Acknowledgments

This work was funded by the Netherlands Organisation for Scientific Research (NWO) within Vici project "Deltas out of shape: regime changes of sediment dynamics in tide-influenced deltas" (Grant NWO-TTW 17062) and Deltares Research Funds. The data presented in this paper stem from the Dutch Rijkswaterstaat, the German Wasserstrassen- und Schifffartsamt (WSA) Ems-Nordsee, and the Niedersächsischer Landesbetrieb für Wasserwirtschaft, Küsten- und Naturschutz (NLWKN). The modelling software Delft3D Flexible Mesh was made available by Deltares via the Delft3D Educational Service Package.

References

Baar, A. W., Boechat Albernaz, M., van Dijk, W. M., & Kleinhans, M. G. (2019). Critical dependence of morphodynamic models of fluvial and tidal systems on empirical downslope sediment transport. *Nature Communications*, *10*(1). Retrieved from http://dx.doi.org/10.1038/s41467-019-12753-x doi: 10.1038/s41467-019-12753-x

Bolla Pittaluga, M., Tambroni, N., Canestrelli, A., Slingerland, R., Lanzoni, S., & Seminara, G. (2015). Where river and tide meet: The morphodynamic equilibrium of alluvial estuaries. *Journal of Geophysical Research: Earth Surface*, *120*(1), 75–94. doi: 10.1002/2014JF003233

Braat, L., Van Kessel, T., Leuven, J. R., & Kleinhans, M. G. (2017). Effects of mud supply on large-scale estuary morphology and development over centuries to millennia. *Earth Surface Dynamics*, *5*(4), 617–652. doi: 10.5194/esurf-5-617-2017

Chen, K., He, Z., Liu, J., Lin, Y., & Jia, L. (2022). Long-term morphological evolution and its mechanism of Lingdingyang Estuary: Interferences from anthropogenic forcings. *Marine Geology*, *450*(June), 106856. Retrieved from https://doi.org/10.1016/j.margeo.2022.106856 doi: 10.1016/j.margeo.2022.106856

Dam, G., Bliek, A. J., Labeur, R. J., Ides, S. J., & Plancke, Y. M. (2008). Long term process-based morphological model of the Western Scheldt Estuary. *River, Coastal and Estuarine Morphodynamics: RCEM 2007 - Proceedings of the 5th IAHR Symposium on River, Coastal and Estuarine Morphodynamics*, *2*(January), 1077–1084. doi: 10.1201/noe0415453639-c135

Dam, G., Van Der Wegen, M., Labeur, R. J., & Roelvink, D. (2016). Modeling centuries of estuarine morphodynamics in the Western Scheldt estuary. *Geophysical Research Letters*, *43*(8), 3839–3847. doi: 10.1002/2015GL066725

Dastgheib, A., Roelvink, J. A., & Wang, Z. B. (2008). Long-term process-based morphological modeling of the Marsdiep Tidal Basin. *Marine Geology*, *256*(1-4), 90–100. Retrieved from http://dx.doi.org/10.1016/j.margeo.2008.10.003 doi: 10.1016/j.margeo.2008.10.003

De Jonge, V. N., Schuttelaars, H. M., van Beusekom, J. E., Talke, S. A., & de Swart, H. E. (2014). The influence of channel deepening on estuarine turbidity levels anddynamics, as exemplified by the Ems estuary. *Estuarine, Coastal and Shelf Science*, *139*, 46–59. doi: 10.1016/j.ecss.2013.12.030

De Swart, H. E., & Zimmerman, J. T. (2009). Morphodynamics of tidal inlet systems. *Annual Review of Fluid Mechanics*, *41*, 203–229. doi: 10.1146/annurev.fluid.010908.165159

De Vriend, H. J., Zyserman, J., Nicholson, J., Roelvink, J. A., Péchon, P., & Southgate, H. N. (1993). Medium-term 2DH coastal area modelling. *Coastal Engineering*, *21*(1-3), 193–224. doi: 10.1016/0378-3839(93)90050-I

Dissanayake, D., Roelvink, J. A., & Van der Wegen, M. (2009). Modelled channel patterns in a schematized tidal inlet. *Coastal Engineering*, *56*(11-12), 1069–1083. Retrieved from http://dx.doi.org/10.1016/j.coastaleng.2009.08.008 doi: 10.1016/j.coastaleng.2009.08.008

Elmilady, H., van der Wegen, M., Roelvink, D., & Jaffe, B. E. (2019). Intertidal Area Disappears Under Sea Level Rise: 250 Years of Morphodynamic Modeling in San Pablo Bay, California. *Journal of Geophysical Research: Earth Surface*, *124*(1), 38–59. doi: 10.1029/2018JF004857

Elmilady, H., Van Der Wegen, M., Roelvink, D., & van der Spek, A. (2020). Morphodynamic Evolution of a Fringing Sandy Shoal : From Tidal Levees to Sea Level Rise. , 1–21. doi: 10.1029/2019JF005397

Elmilady, H., van der Wegen, M., Roelvink, D., & van der Spek, A. (2022). Modeling the Morphodynamic Response of Estuarine Intertidal Shoals to Sea-Level Rise. *Journal of Geophysical Research: Earth Surface*, *127*(1), 1–26. doi:

10.1029/2021JF006152
Friedrichs, C. T. (2011). *Tidal Flat Morphodynamics: A Synthesis* (Vol. 3). Elsevier Inc. Retrieved from http://dx.doi.org/10.1016/B978-0-12-374711-2.00307-7 doi: 10.1016/B978-0-12-374711-2.00307-7
Friedrichs, C. T., & Aubrey, D. G. (1988). Nonlinear tidal distortion in shallow well-mixed estuaries. *Estuarine, Coastal and Shelf Science*, *30*(3), 321–322. doi: 10.1016/0272-7714(90)90054-U
Ganju, N. K., Jaffe, B. E., & Schoellhamer, D. H. (2011). Discontinuous hindcast simulations of estuarine bathymetric change: A case study from Suisun Bay, California. *Estuarine, Coastal and Shelf Science*, *93*(2), 142–150. Retrieved from http://dx.doi.org/10.1016/j.ecss.2011.04.004 doi: 10.1016/j.ecss.2011.04.004
Ganju, N. K., & Schoellhamer, D. H. (2010). Decadal-timescale estuarine geomorphic change under future scenarios of climate and sediment supply. *Estuaries and Coasts*, *33*(1), 15–29. doi: 10.1007/s12237-009-9244-y
Ganju, N. K., Schoellhamer, D. H., & Jaffe, B. E. (2009). Hindcasting of decadal-timescale estuarine bathymetric change with a tidal-timescale model. *Journal of Geophysical Research: Earth Surface*, *114*(4). doi: 10.1029/2008JF001191
Geleynse, N., Storms, J. E., Walstra, D. J. R., Jagers, H. R., Wang, Z. B., & Stive, M. J. (2011). Controls on river delta formation; insights from numerical modelling. *Earth and Planetary Science Letters*, *302*(1-2), 217–226. Retrieved from http://dx.doi.org/10.1016/j.epsl.2010.12.013 doi: 10.1016/j.epsl.2010.12.013
George, D. A., Gelfenbaum, G., & Stevens, A. W. (2012). Modeling the Hydrodynamic and Morphologic Response of an Estuary Restoration. *Estuaries and Coasts*, *35*(6), 1510–1529. doi: 10.1007/s12237-012-9541-8
Guo, L., van der Wegen, M., Roelvink, D., & He, Q. (2015). Exploration of the impact of seasonal river discharge variations on long-term estuarine morphodynamic behavior. *Coastal Engineering*, *95*, 105–116. Retrieved from http://dx.doi.org/10.1016/j.coastaleng.2014.10.006 doi: 10.1016/j.coastaleng.2014.10.006
Guo, L., Wegen, M. v. d., Wang, Z. B., Roelvink, D., & He, Q. (2016). Exploring the impacts of multiple tidal constituents and varying river flow on long-term, large-scale estuarine morphodynamics by means of a 1-D model. *Journal of Geophysical Research: Earth Surface*, *121*, 1000–1022. doi: doi:10.1002/2016JF003821
He, Z., Liang, M., Jia, L., Dong, H., Chen, K., Liu, J., … Ou, J. (2022). Long-term morphological modeling and implication for estuarine regulation of the Modaomen Estuary, Pearl River Delta, China. *Applied Ocean Research*, *123*(October 2021), 103184. Retrieved from https://doi.org/10.1016/j.apor.2022.103184 doi: 10.1016/j.apor.2022.103184
Hibma, a., de Vriend, H., & Stive, M. (2003, 8). Numerical modelling of shoal pattern formation in well-mixed elongated estuaries. *Estuarine, Coastal and Shelf Science*, *57*(5-6), 981–991. Retrieved from http://linkinghub.elsevier.com/retrieve/pii/S0272771403000040 doi: 10.1016/S0272-7714(03)00004-0
Hoitink, A. J., Hoekstra, P., & Van Maren, D. S. (2003). Flow asymmetry associated with astronomical tides: Implications for the residual transport of sediment. *Journal of Geophysical Research: Oceans*, *108*(10), 1–8. doi: 10.1029/2002jc001539
Hoitink, A. J., Nittrouer, J. A., Passalacqua, P., Shaw, J. B., Langendoen, E. J., Huismans, Y., & van Maren, D. S. (2020). Resilience of River Deltas in the Anthropocene. *Journal of Geophysical Research: Earth Surface*, *125*(3), 1–24. doi: 10.1029/2019JF005201
Kernkamp, H. W. J., Van Dam, A., Stelling, G. S., & De Goede, E. D. (2011).

Efficient scheme for the shallow water equations on unstructured grids with application to the Continental Shelf. *Ocean Dynamics*, *61*(8), 1175–1188. doi: 10.1007/s10236-011-0423-6

Latteux, B. (1995). Techniques for long-term morphological simulation under tidal action. *Marine Geology*, *126*(1-4), 129–141. Retrieved from `http://dx.doi.org/10.1016/0025-3227(95)00069-B` doi: 10.1016/0025-3227(95)00069-B

Leonardi, N., Canestrelli, A., Sun, T., & Fagherazzi, S. (2013). Effect of tides on mouth bar morphology and hydrodynamics. *Journal of Geophysical Research: Oceans*, *118*(9), 4169–4183. doi: 10.1002/jgrc.20302

Lesser, G. (2009). *An Approach to Medium-term Coastal Morphological Modelling.* Retrieved from `http://www.narcis.nl/publication/RecordID/oai:tudelft.nl:uuid:62caa573-4fc0-428e-8768-0aa47ab612a9`

Luan, H. L., Ding, P. X., Wang, Z. B., & Ge, J. Z. (2017). Process-based morphodynamic modeling of the Yangtze Estuary at a decadal timescale: Controls on estuarine evolution and future trends. *Geomorphology*, *290*(April), 347–364. Retrieved from `http://dx.doi.org/10.1016/j.geomorph.2017.04.016` doi: 10.1016/j.geomorph.2017.04.016

Marciano, R., Wang, Z. B., Hibma, A., De Vriend, H. J., & Defina, A. (2005). Modeling of channel patterns in short tidal basins. *Journal of Geophysical Research: Earth Surface*, *110*(1), 1–13. doi: 10.1029/2003JF000092

Nahon, A., Bertin, X., Fortunato, A. B., & Oliveira, A. (2012). Process-based 2DH morphodynamic modeling of tidal inlets: A comparison with empirical classifications and theories. *Marine Geology*, *291-294*, 1–11. Retrieved from `http://dx.doi.org/10.1016/j.margeo.2011.10.001` doi: 10.1016/j.margeo.2011.10.001

Nidzieko, N. J., & Ralston, D. K. (2012). Tidal asymmetry and velocity skew over tidal flats and shallow channels within a macrotidal river delta. *Journal of Geophysical Research: Oceans*, *117*(3), 1–17. doi: 10.1029/2011JC007384

Nnafie, A., de Swart, H. E., De Maerschalck, B., Van Oyen, T., van der Vegt, M., & van der Wegen, M. (2019). Closure of Secondary Basins Causes Channel Deepening in Estuaries With Moderate to High Friction. *Geophysical Research Letters*, *46*(22), 13209–13216. doi: 10.1029/2019GL084444

Nnafie, A., Van Oyen, T., De Maerschalck, B., van der Vegt, M., & van der Wegen, M. (2018). Estuarine Channel Evolution in Response to Closure of Secondary Basins: An Observational and Morphodynamic Modeling Study of the Western Scheldt Estuary. *Journal of Geophysical Research: Earth Surface*, *123*(1), 167–186. doi: 10.1002/2017JF004364

Pawlowicz, R., Beardsley, B., & Lentz, S. (2002). Classical tidal harmonic analysis including werror estimates in MATLAB using T_TIDE. *Computers and Geosciences*, *28*(8), 929–937. doi: 10.1016/S0098-3004(02)00013-4

Pugh, D. T. (1987). *Tides, surges and mean sea level.* Swindon, UK: John Wiley and Sons Ltd. Retrieved from `https://www.osti.gov/biblio/5061261`

Ranasinghe, R., Swinkels, C., Luijendijk, A., Roelvink, D., Bosboom, J., Stive, M., & Walstra, D. J. (2011). Morphodynamic upscaling with the MORFAC approach: Dependencies and sensitivities. *Coastal Engineering*, *58*(8), 806–811. Retrieved from `http://dx.doi.org/10.1016/j.coastaleng.2011.03.010` doi: 10.1016/j.coastaleng.2011.03.010

Reyns, J., Dastgheib, A., Ranasinghe, R., Luijendijk, A., Walstra, D.-J., & Roelvink, D. (2014). Morphodynamic Upscaling With the Morfac Approach in Tidal Conditions: the Critical Morfac. *Coastal Engineering Proceedings*, *1*(34), 27. doi: 10.9753/icce.v34.sediment.27

Roelvink, D. (2006). Coastal morphodynamic evolution techniques. *Coastal Engineering*, *53*(2-3), 277–287. doi: 10.1016/j.coastaleng.2005.10.015

Roelvink, D., & Reniers, A. (2011). *A Guide to Modeling Coastal Morphology* (Advances i ed.). WORLD SCIENTIFIC. Retrieved from `https://`

`www.worldscientific.com/doi/abs/10.1142/7712` doi: 10.1142/7712

Song, D., Wang, X. H., Kiss, A. E., & Bao, X. (2011). The contribution to tidal asymmetry by different combinations of tidal constituents. *Journal of Geophysical Research: Oceans*, *116*(12), 1–12. doi: 10.1029/2011JC007270

Styles, R., Brown, M. E., Brutsché, K. E., Li, H., Beck, T. M., & Sánchez, A. (2016). Long-term morphological modeling of barrier island tidal inlets. *Journal of Marine Science and Engineering*, *4*(4). doi: 10.3390/jmse4040065

Syvitski, J. P., Kettner, A. J., Overeem, I., Hutton, E. W., Hannon, M. T., Brakenridge, G. R., ... Nicholls, R. J. (2009). Sinking deltas due to human activities. *Nature Geoscience*, *2*(10), 681–686. doi: 10.1038/ngeo629

Van de Kreeke, J., & Robaczewska, K. (1993). Tide-induced residual transport of coarse sediment; Application to the EMS estuary. *Netherlands Journal of Sea Research*, *31*(3), 209–220. doi: 10.1016/0077-7579(93)90022-K

Van der Wegen, M., Dastgheib, A., & Roelvink, J. A. (2010). Morphodynamic modeling of tidal channel evolution in comparison to empirical PA relationship. *Coastal Engineering*, *57*(9), 827–837. Retrieved from `http://dx.doi.org/10.1016/j.coastaleng.2010.04.003` doi: 10.1016/j.coastaleng.2010.04.003

Van der Wegen, M., & Jaffe, B. E. (2013). Towards a probabilistic assessment of process-based, morphodynamic models. *Coastal Engineering*, *75*, 52–63. Retrieved from `http://dx.doi.org/10.1016/j.coastaleng.2013.01.009` doi: 10.1016/j.coastaleng.2013.01.009

Van der Wegen, M., & Jaffe, B. E. (2014). Processes governing decadal-scale depositional narrowing of the major tidal channel in San Pablo Bay, California, USA. *Journal of Geophysical Research F: Earth Surface*(119), 1136–1154. doi: doi:10.1002/2013JF002824

Van Der Wegen, M., Jaffe, B. E., & Roelvink, J. A. (2011). Process-based, morphodynamic hindcast of decadal deposition patterns in San Pablo Bay, California, 1856-1887. *Journal of Geophysical Research: Earth Surface*, *116*(2), 1–22. doi: 10.1029/2009JF001614

Van der Wegen, M., & Roelvink, J. A. (2008). Long-term morphodynamic evolution of a tidal embayment using a two-dimensional, process-based model. *Journal of Geophysical Research: Oceans*, *113*(3), 1–23. doi: 10.1029/2006JC003983

Van der Wegen, M., & Roelvink, J. A. (2012). Reproduction of estuarine bathymetry by means of a process-based model: Western Scheldt case study, the Netherlands. *Geomorphology*, *179*, 152–167. Retrieved from `http://dx.doi.org/10.1016/j.geomorph.2012.08.007` doi: 10.1016/j.geomorph.2012.08.007

Van der Wegen, M., Van der Werf, J., De Vet, L., & Robke, B. (2017). *Hindcasting Westerschelde mouth morphodynamics (1963-2011)* (Tech. Rep.).

Van der Wegen, M., Wang, Z., Savenije, H. H., & Roelvink, J. A. (2008). Long-term morphodynamic evoluation and energy dissipation in a coastal plain, tidal embayment. *Journal of Geophysical Research: Earth Surface*, *113*(3), 1–22. doi: 10.1029/2007JF000898

Van Maanen, B., Coco, G., & Bryan, K. (2011). A numerical model to simulate the formation and subsequent evolution of tidal channel networks. *Australian Journal of Civil Engineering*, *9*(1), 61–72. doi: 10.1080/14488353.2011.11463969

Van Maanen, B., Coco, G., & Bryan, K. R. (2013). Modelling the effects of tidal range and initial bathymetry on the morphological evolution of tidal embayments. *Geomorphology*, *191*, 23–34. Retrieved from `http://dx.doi.org/10.1016/j.geomorph.2013.02.023` doi: 10.1016/j.geomorph.2013.02.023

Van Maren, D. S., & Gerritsen, H. (2012). Residual flow and tidal asymmetry in the Singapore Strait, with implications for resuspension and residual transport of sediment. *Journal of Geophysical Research: Oceans*, *117*(4), 1–18. doi: 10.1029/2011JC007615

Van Maren, D. S., Hoekstra, P., & Hoitink, A. J. (2004). Tidal flow asymmetry in the diurnal regime: bed-load transport and morphologic changes around the Red River Delta. (January). doi: 10.1007/s10236-003-0085-0

Van Maren, D. S., Winterwerp, J. C., & Vroom, J. (2015). Fine sediment transport into the hyper-turbid lower Ems River: the role of channel deepening and sediment-induced drag reduction. *Ocean Dynamics*, *65*(4), 589–605. doi: 10.1007/s10236-015-0821-2

Van Rijn, L. C. (1993). Principles of sediment transport in rivers, estuaries and coastal seas..

Weisscher, S. A., Baar, A. W., van Belzen, J., Bouma, T. J., & Kleinhans, M. G. (2022). Transitional polders along estuaries: Driving land-level rise and reducing flood propagation. *Nature-Based Solutions*, *2*(June), 100022. Retrieved from `https://doi.org/10.1016/j.nbsj.2022.100022` doi: 10.1016/j.nbsj.2022.100022

Xie, D., Gao, S., Wang, Z. B., Pan, C., Wu, X., & Wang, Q. (2017). Morphodynamic modeling of a large inside sandbar and its dextral morphology in a convergent estuary: Qiantang Estuary, China. *Journal of Geophysical Research: Earth Surface*, *122*(8), 1553–1572. doi: 10.1002/2017JF004293

Yu, Q., Wang, Y., Flemming, B., & Gao, S. (2014). Scale-dependent characteristics of equilibrium morphology of tidal basins along the Dutch-German North Sea Coast. *Marine Geology*, *348*, 63–72. Retrieved from `http://dx.doi.org/10.1016/j.margeo.2013.12.005` doi: 10.1016/j.margeo.2013.12.005

Zhang, S., & Mao, X. z. (2015). Hydrology, sediment circulation and long-term morphological changes in highly urbanized Shenzhen River estuary, China: A combined field experimental and modeling approach. *Journal of Hydrology*, *529*, 1562–1577. Retrieved from `http://dx.doi.org/10.1016/j.jhydrol.2015.08.027` doi: 10.1016/j.jhydrol.2015.08.027

Zheng, J., Elmilady, H., Röbke, B., Taal, M., Wang, Z., Prooijen, B., . . . Wegen, M. (2021). The impact of wind-waves and sea level rise on the morphodynamics of a sandy estuarine shoal. *Earth Surface Processes and Landforms*(November 2020), 1–18. doi: 10.1002/esp.5207

Zhou, Z., Coco, G., Jimenez, B., Olabarrieta, M., Van der Wegen, M., & Townend, I. (2014). Morphodynamics of river-influenced back-barrier tidal basins: The role of landscape and hydrodynamic settings. *Water Resources Research*(50), 3826–3851. doi: 10.1002/2014WR015891.Received

Zijl, F., & Groenenboom, J. (2019). *Development of a sixth generation model for the NW European Shelf (DCSM-FM 100m)* (Tech. Rep.). Delft, The Netherlands: Deltares.